Safety, Reliability and Risk of Structures, Infrastructures and Engineering Systems – Furuta, Frangopol & Shinozuka (eds)
© 2010 Taylor & Francis Group, London, ISBN 978-0-415-47557-0

Use of digital aerial camera images to detect damage to an expressway following an earthquake

Yoshihisa Maruyama & Fumio Yamazaki
Department of Urban Environment Systems, Chiba University, Chiba, Japan.

ABSTRACT: A new procedure using digital aerial images for detecting damage to an expressway following an earthquake is presented. Remotely sensed image data from satellites and airborne platforms are important for understanding the distribution of damage due to large earthquakes. Digital aerial images captured by air survey companies following the 2004 Mid-Niigata earthquake in Japan were used for the detection of damage to expressway. The results of image processing using analog and digital aerial images were compared. The effectiveness of the new procedure in detect damage is shown to be excellent, with nearly all damage detected.

1 INTRODUCTION

Remotely sensed data obtained from satellites and airborne platforms are useful in providing an understanding of the distribution of damage due to natural disasters (Yamazaki 2001). The platforms and sensors of remote sensing should be selected with regards to the coverage and resolution required and the urgency, weather and time conditions. QuickBird is a high-resolution commercial satellite with a maximum spatial resolution of 0.6 m and was launched on October 18, 2001. QuickBird images can be used to detect damage to individual buildings following natural disasters (Kouchi *et al.* 2003; Yano *et al.* 2004; Miura & Midorikawa 2008).

Expressways play an important role in providing access for restoration work in damaged areas, and it is necessary to keep the duration of functional loss to a minimum. In the Mid-Niigata earthquake, October 23, 2004, both major and minor damage caused expressways to be closed, and the regular four-lane road was only reopened after about a month (Maruyama *et al.* 2007).

Aerial photography is useful for the detection of damages due to earthquakes due to its very high resolution (Yamazaki *et al.* 2008). Maruyama *et al.* (2006) attempted to detect expressway damages after the 2004 Mid-Niigata earthquake using image processing of analog aerial photographs. The aerial photos used in the study were taken by Geographic Survey Institute of Japan following the earthquake. The analog aerial photographs were digitized by film scanner and then put through image processing.

Recently, the digital mapping camera system (DMC) has become widely used (Hinz 1999; Leberl & Gruber 2005). The DMC saves time associated with analog imagery processes and provides more precise and better-quality aerial images. In addition, the DMC has a near infrared (NIR) band, which can be used for extraction of vegetated areas, which can be used to assess expressway damage. The method proposed by the authors (Maruyama *et al.* 2006) did not consider the vegetation near the expressway.

In this study, digital aerial camera images are used to detect expressway damage caused during the 2004 Mid-Niigata earthquake. Firstly, a conventional pixel-based classification was conducted for both the analog and digital image for comparison purposes in chapter 2. Secondly, the procedure proposed by this study was performed in order to detect expressway damages. The results of image processing using scanned-analog (section 3.1) and digital aerial images (section 3.2) were compared. A new methodology for detecting damages using digital aerial images is presented in section 3.3. The accuracy of the damage estimation and the effectiveness of our me-

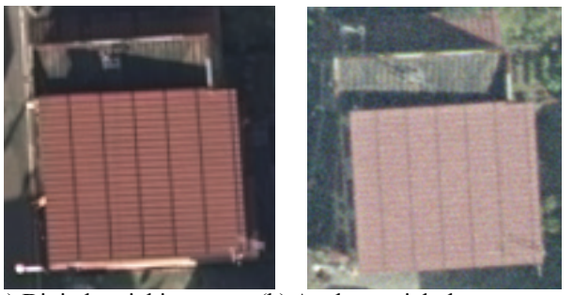

(a) Digital aerial image (108×113 pixels) (b) Analog aerial photo (167×187 pixels)

Figure 1. Comparison of (a) digital and (b) analog aerial images captured after the 2004 Mid-Niigata earthquake.

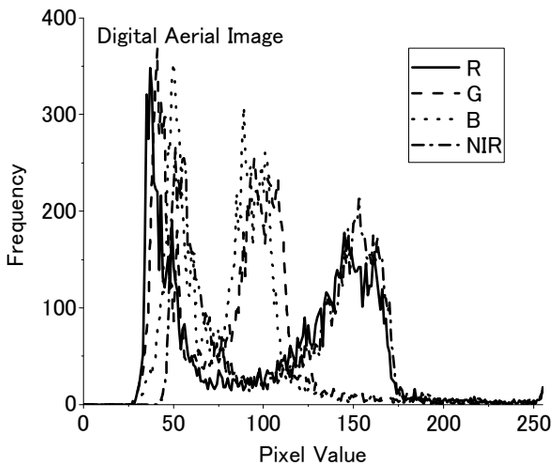

(a) Digital aerial image

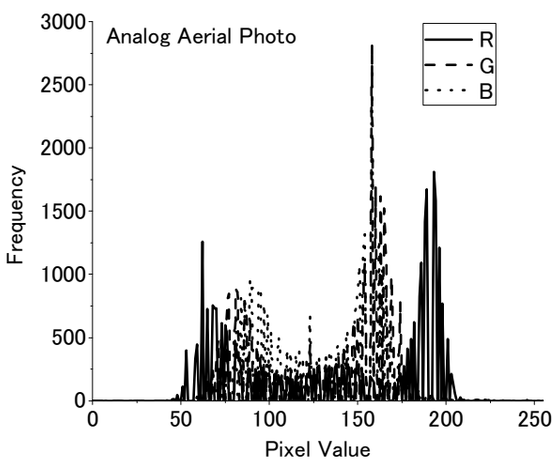

(b) Analog aerial image

Figure 2. Histograms of pixel values of (a) digital and (b) analog aerial images shown in Figure 1

thod are discussed with comparison to actual damage data.

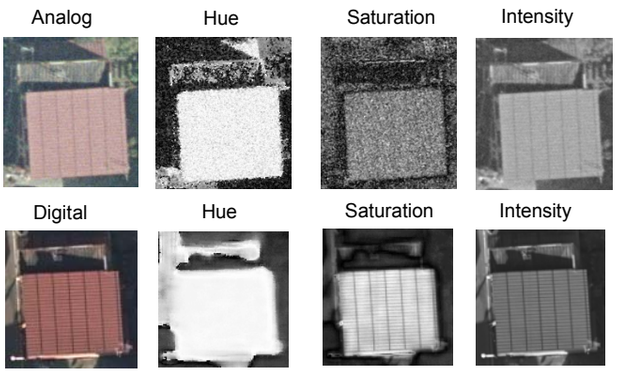

Figure 3. HSI transformation of the (a) analog and (b) digital aerial images.

Figure 4. Comparison of the (a) digital and (b) analog aerial images showing the damaged section of the expressway.

2 COMPARISON BETWEEN DIGITAL AND ANALOG AERIAL IMAGES

Analog aerial photographs are composed of three visible bands (Red, Green and Blue). Digital aerial cameras also have a near infrared (NIR) band. The detection of vegetation using the NIR band is simple. Digital aerial cameras also have much higher radiometric resolution than analog aerial cameras, providing a clearer image of the earth's surface at the same spatial resolution.

Figure 1 shows the roof of a wooden house captured by both digital and analog aerial cameras in Kawaguchi town, Niigata, which was subject to severe ground motion during the Mid-Niigata earthquake (Honda *et al.* 2005). The Geographical Survey Institute, Japan, took analog aerial photos on the morning of October 24, 2004 (one day after the earthquake) and Asia Air Survey Co., Ltd. obtained digital aerial images using DMC on the afternoon of the same day. Some salt-and-pepper noise is present in the analog aerial photo although there are more pixels than in the digital image. Figure 2 shows the histogram of pixel values of the two images in Figure 1. The pixel values of the digital aerial image are distributed from about 25 to 200 without any gaps, whilst those of analog image show discontinuities

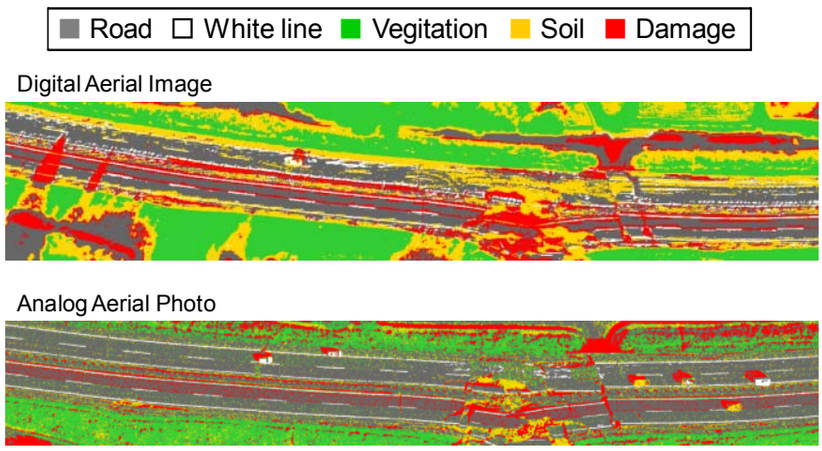

Figure 5. Results of the pixel-based classification based on the maximum likelihood method for digital and analog aerial images.

due to analog-digital conversion. The discontinuous distribution of pixel values results in a smudged appearance of the image.

HSI (Hue, Saturation and Intensity) are related representation of points in an RGB color space, used to describe perceptual color relationships more accurately than RGB (Mitomi *et al.* 2001). H, S and I are defined as:

$$H = \tan^{-1}(C_1/C_2) \tag{1}$$

$$S = \sqrt{C_1^2 + C_2^2} \tag{2}$$

$$I = 0.3R + 0.59G + 0.11B \tag{3}$$

where $C_1 = R - I$ and $C_2 = B - I$, respectively. Figure 3 shows the HSI transformation of the two images in Figure 1. As expected, the results show the presence of salt-and-pepper noise for hue and saturation in the analog aerial image.

Figure 4 shows the damaged section of the expressway captured by digital and analog aerial images following the 2004 Mid-Niigata earthquake. Assuming the availability of proper training data, a conventional pixel-based classification was carried out based on the maximum likelihood method, the most common supervised classification method. Figure 5 shows the classification results for the two images. Salt-and-pepper noise was still present after processing the analog photo, but less noise was present in the processed digital aerial image. Detection of vegetated areas was simple for the digital image because it has a NIR band.

The damage to the expressway using the pixel-based classification technique was detected as shadow. The damage was effectively detected in the digital aerial image, except where the shadow of trees is misinterpreted as damage in the left part of the image. However, it is necessary to prepare suitable training datasets to achieve a reasonable result by pixel-based classification. If a wider area is covered by the aerial image, different types of land cover classes may be present and more training data is required. From the viewpoint of an emergency response following an earthquake, a damage detection technique with less pre-processing is preferable.

3 DETECTION OF DAMAGE TO THE EXPRESSWAY USING IMAGE PROCESSING

3.1 *Result using an analog aerial photograph*

Maruyama *et al.* (2006) attempted to detect damaged sections of the expressway according to the procedure in Figure 6. Before performing the procedure, the image was smoothed by median filter with a 3 x 3 pixel window (Parker 1997). The median filter was applied to the image five times in order to reduce the salt-and-pepper_noise in the results. HSI transformation was conducted, then the brightness (intensity) image was used for image processing. Pixels on the road surface were removed based on a differential operation using the Sobel filter with a 3 x 3 pixel window (Parker 1997), since the change of intensity between pixels on the road surface is small. Then, the direction of the expressway was estimated from the histogram of edge angles. The centerlines and lane lines were then eliminated as road components. The damaged sections of the expressway were then detected. Figure 7 shows an example of damage detection performed by the authors (Maruyama *et al.* 2006)

Figure 8 compares results of damage detection between visual inspection and image processing using the analog aerial photograph. Since vegetated areas were disregarded in the analytical flow (Figure 6), the vegetation near the expressway was recognized as damage. Although the image was smoothed by the median filter, some noise remains in the result.

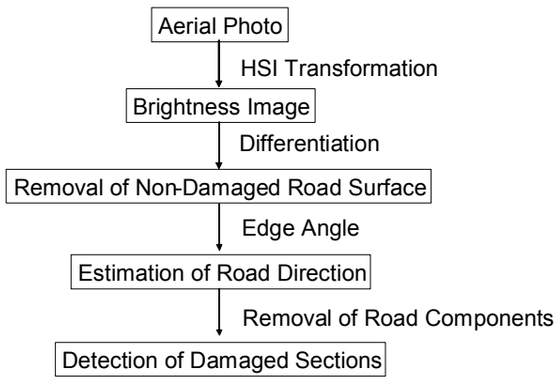

Figure 6. Flowchart of image processing used to detect damaged sections of expressway proposed by Maruyama *et al.* (2006).

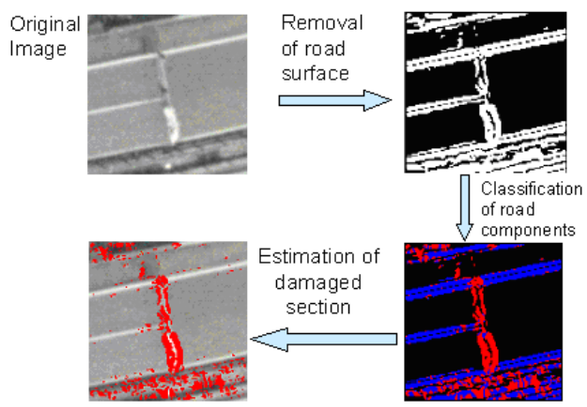

Figure 7. Example of the analytical flow used to detect damaged sections of expressway.

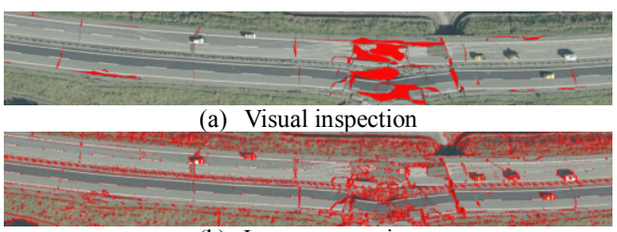

(a) Visual inspection

(b) Image processing

Figure 8. Comparison of the detection of expressway damage between (a) visual damage inspection and (b) image processing using the analog aerial photograph.

These two issues will be resolved using the digital aerial image.

3.2 *Image processing of digital aerial image*

The digital aerial image provided by Asia Air Survey Co., Ltd. was put through image processing in order to detect expressway damage. Following the same procedure described above, the median filter with a 3 x 3 pixel window was applied to the digital aerial image five times. Then, the differential operation was performed by applying the Sobel filter. According to the histogram of differential values obtained from the road surface (Figure 9), the pixels of road

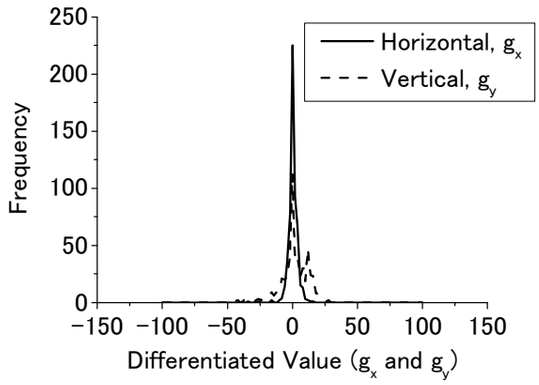

Figure 9. Histogram of differentiated values for horizontal and vertical directions obtained from the road surface of the digital aerial image.

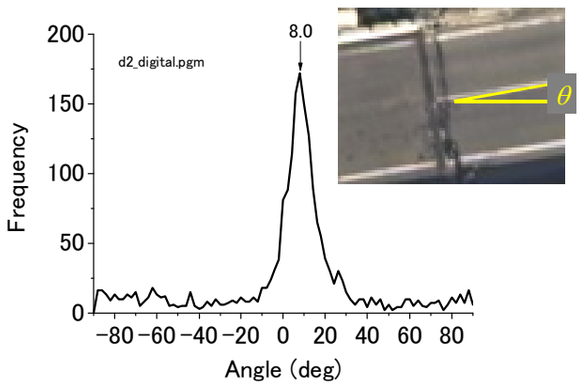

Figure 10. Histogram of edge angles obtained from the digital aerial image.

surface were identified as

$$(|g_x| < c) \cap (|g_y| < c) \tag{4}$$

where g_x and g_y are horizontally and vertically differentiated values, respectively, and c is the threshold value to identify the road surface, which is set at 25 (Figure 9).

After removing the road surface pixels, the edge angle was calculated by Eq. (5).

$$\theta = \arctan(g_x / g_y) \tag{5}$$

The direction of the road angle was determined from the histogram of the edge angles (Figure 10). If the edge angle was in a range of ten degrees centered at the mode, the pixel was considered to be a road component, such as the centerline.

Pixels not classified as road surface or road components were regarded as damages induced by earthquake. Figure 11 shows an example of damage detected using the digital aerial image, following the same procedure as used on the analog aerial photograph. The result shows that only a part of damage was extracted by image processing. The result from the analog aerial photo indicated the damage more

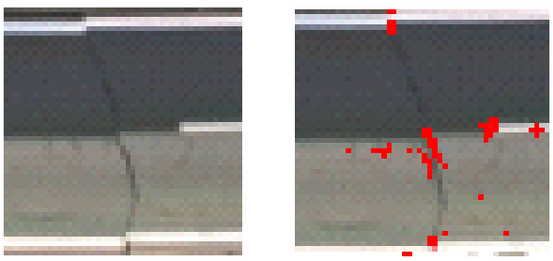

(a) Original digital image (b) Estimated damage

Figure 11. Example of image processing including smoothing by the median filter for the digital aerial image (a) original digital image and (b) estimated damage in red pixels.

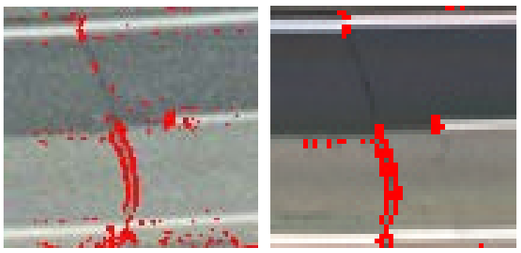

(a)Analog aerial photo (b) Digital aerial image

Figure 12. Result of image processing for detection of damage (red pixels) for the (a) analog and (b) digital aerial images, where the median filter is not applied to the digital aerial image.

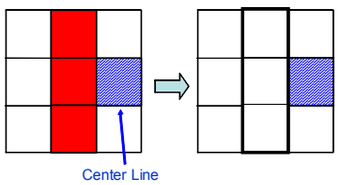

(a) Error adjacent to the center line

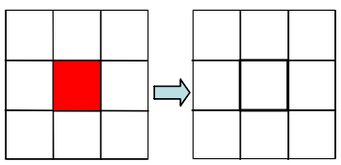

(b) Error in an individual pixel

Figure 13. The rules to reduce error in the detection of damage (a) adjacent to the center line and (b) in individual pixels.

precisely despite some remaining noise (Figure 12(a)). Figure 12(b) shows the result from the digital image without application of the median filter. Whilst the median filter was effective in smoothing the analog image, it reduced the accuracy of damage detection in the digital aerial image. Hence, the median filter was not employed for the digital aerial image.

Since no smoothing process was performed, individual pixels were sometimes misinterpreted as expressway damage. In addition, the end of the centerline was also misinterpreted as damage since it has

(a)Original digital aerial image

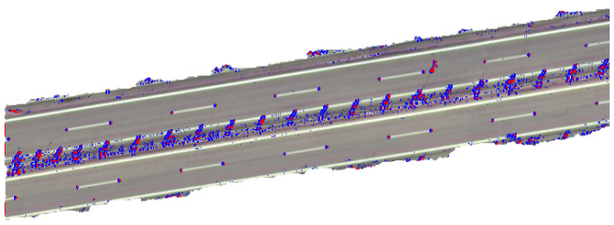

(b) Result of image processing

Figure 14. The result of image processing for non-damaged section of expressway. The blue pixels show the result of image processing before removing the errors and the red pixels are obtained after removing the errors.

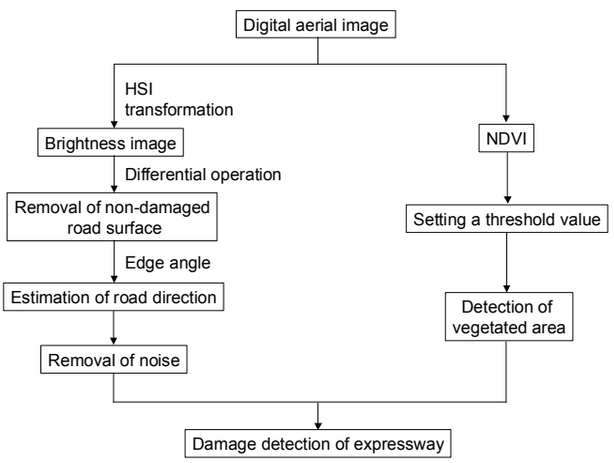

Figure 15. Flowchart of proposed method for detection of expressway damage using digital aerial images.

an edge angle perpendicular to the road angle. To reduce these errors, two rules were applied in image processing, as shown in Figure 13. Firstly, if the pixel lay beside the centerline, it was not regarded as road damage (Figure 13(a)), and secondly, if only one pixel was recognized as damage in a 3 x 3 pixel window, the result was assumed to be an error (Figure 13(b)).

The effects of these rules were assessed through a series of image processing performed on a non-damaged section of the expressway. Figure 14 shows the original digital aerial image and the result of image processing. The blue pixels were misinterpreted as damage before the errors were removed. The red pixels show the result of image processing after applying the two rules. Some errors remain, however, the rules are effective in improving the accuracy of the result.

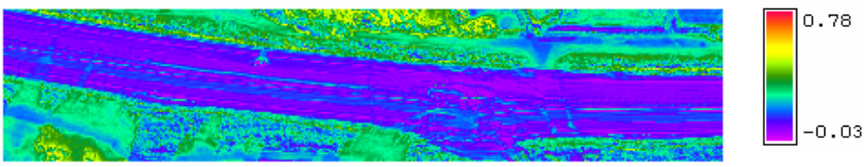

Figure 16. NDVI values for the digital aerial image showing the expressway.

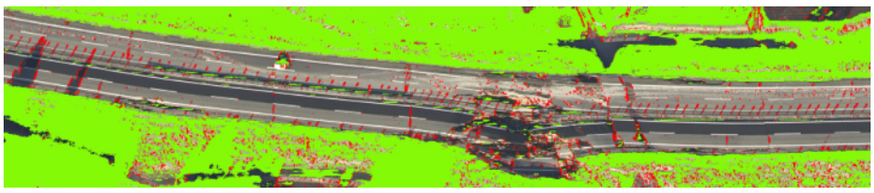

(a) Result of image processing

(b) Result of visual inspection

Figure 17. Comparison of the results of (a) image processing of the digital aerial image and (b) visual damage inspection. Damage to the expressway is shown in red.

3.3 *Extended method to detect expressway damage using digital aerial image*

An extended analytical procedure for the detection of expressway damage using digital aerial images is proposed, based on the methods presented in the previous section. Figure 15 shows a flowchart describing the automated damage detection technique.

In order to detect vegetated areas, the normalized vegetation index (NDVI) is calculated by Eq. (6) (Campbell 2006).

$$NDVI = \frac{NIR - R}{NIR + R} \tag{6}$$

NDVI is a simple and reliable index used to identify the presence of growing vegetation and is widely applied. Figure 16 illustrates the NDVI values for the digital image. The vegetated areas were masked before image processing using a NDVI threshold value of 0.20.

The median filter was not used in the image processing of the digital aerial image, instead, the errors adjacent to the centerlines and in individual pixels were identified according to the rules given above, and included in the procedure shown in Figure 15. Figure 17 compares the result of image processing with that of visual damage inspection. Almost all damaged sections of the expressway were properly detected through the series of image processing outlined in this study.

The method proposed in this study does not, however, consider shadows, and the correction of brightness in the portion of the image in shadow is desirable for more accurate results.

4 CONCLUSIONS

This study proposes a new procedure to identify damaged sections of expressway following an earthquake using a digital aerial image. The same procedure as proposed by Mayuyama *et al* (2006) using analog aerial photo was applied to the digital image. A comparison of the results obtained from the digital and analog aerial images was used to propose an extended methodology for the digital image.

Smoothing using the median filter was not required due to the characteristics of pixel values in the digital aerial image. Errors adjacent to the centerlines and in individual pixels tended to be generated when no smoothing process was used. These errors were removed using rules.

Using the new procedure, almost all the damaged sections of the expressway were properly detected. In order to improve the accuracy of damage detection, the effects of shadow should be taken into account. The obtained results will be helpful for a rapid earthquake response by highway authorities.

REFERENCES

Campbell J.B. 2006. *Introduction to Remote Sensing*, Taylor & Francis.

Hinz, A. 1999. The Z/I digital aerial camera system, *Proceedings of the 47th Photogrammetric Week 1999*, 109-115.

Honda, R., Aoi, S., Morikawa, N., Sekiguchi, H. Kunugi, T. & Fujiwara, H. 2005. Ground motion and rupture process of the 2004 Mid Niigata Prefecture earthquake obtained from strong motion data of K-NET and KiK-net, *Earth Planets Space*, 57, 527–532.

Kouchi, K., Yamazaki, F., Kohiyama, M., Matsuoka, M. & Muraoka, N. 2004. Damage Detection from QuickBird High-resolution Satellite Images for the 2003 Boumerdes, Algeria Earthquake. *Proceedings of the Asia Conference on Earthquake Engineering*, CD-ROM, 215-226.

Leberl, F. & Gruber, M. 2005. ULTRACAM-D: Understanding some Noteworthy Capabilities, *Proceedings of the 53th Photogrammetric Week 05*, 57-68.

Maruyama, Y. Yamazaki, F., Yogai, H. & Tsuchiya, Y. 2007. Relationship between damage ratio of expressway embankment and seismic intensity in the 2004 Mid-Niigata earthquake. *Proceedings of the 8th Pacific Conference on Earthquake Engineering*, CD-ROM, Paper No. 055.

Maruyama, Y., Yamazaki, F., Yogai, H. & Tsuchiya, Y. 2006. Interpretation of expressway damages in the 2004 mid Niigata earthquake based on aerial photographs. *Proceedings of the First European Conference on Earthquake Engineering and Seismology*, CD-ROM, 8p, Paper No. 738.

Mitomi, H., Yamazaki, F. & Matsuoka, M. 2001. Development of automated extraction method for building damage area based on maximum likelihood classifier. *Proceedings of the 8th International Conference on Structural Safety and Reliability*, CD-ROM, 8p.

Miura, H. & Midorikawa, S. 2008. Detection of Slope Failure Areas Using High-Resolution Satellite Images and Digital Elevation Model for the 2004 Niigata-Ken Chuetsu, Japan Earthquake. *Proceedings of 5th International Conference on Urban Earthquake Engineering*, 559-564.

Parker J.R. 1997. *Algorithms for Image Processing and Computer Vision*, Wiley.

Yamazaki, F. 2001. Applications of remote sensing and GIS for damage assessment. *Proceedings of the 8th International Conference on Structural Safety and Reliability*, CD-ROM, 12p.

Yamazaki, F., Suzuki, D. & Maruyama, Y. 2008. Use of Digital Aerial Images to Detect Damages Due to Earthquakes. *Proceedings of the 14th World Conference on Earthquake Engineering*, Paper-ID 01-1049, CD-ROM, 8p.

Yano, Y., Yamazaki, F., Matsuoka, M. & Vu, T. T. 2004. Building Damage Detection of the 2003 Bam, Iran Earthquake Using QuickBird Images. *Proceedings of the 25th Asian Conference on Remote Sensing*, CD-ROM, 618-623.